

# RSC Advances



This is an *Accepted Manuscript*, which has been through the Royal Society of Chemistry peer review process and has been accepted for publication.

*Accepted Manuscripts* are published online shortly after acceptance, before technical editing, formatting and proof reading. Using this free service, authors can make their results available to the community, in citable form, before we publish the edited article. This *Accepted Manuscript* will be replaced by the edited, formatted and paginated article as soon as this is available.

You can find more information about *Accepted Manuscripts* in the [Information for Authors](#).

Please note that technical editing may introduce minor changes to the text and/or graphics, which may alter content. The journal's standard [Terms & Conditions](#) and the [Ethical guidelines](#) still apply. In no event shall the Royal Society of Chemistry be held responsible for any errors or omissions in this *Accepted Manuscript* or any consequences arising from the use of any information it contains.

# Synthesis of Er<sup>3+</sup>/Yb<sup>3+</sup> codoped NaMnF<sub>3</sub> nanocubes with single-band red upconversion luminescence

Zhenhua Bai,<sup>a</sup> Hui Lin,<sup>b</sup> Kenji Imakita,<sup>b</sup> Reza Montazami,<sup>a</sup> Minoru Fujii<sup>b</sup> and Nastaran Hashemi<sup>\*a</sup>

## Abstract

We have developed a facile low-temperature synthetic method for the preparation of NaMnF<sub>3</sub> nanocubes with Er<sup>3+</sup> and Yb<sup>3+</sup> ions homogeneously incorporated in the host lattice. The effects of the reaction temperature, and the volume ratio between ethanol and DI water on morphology of NaMnF<sub>3</sub> nanocubes are systematically investigated. The NaMnF<sub>3</sub> nanocubes can be produced in the low temperature range (25~80 °C), and the higher reaction temperature (80 °C) is favorable for the formation of smooth surface. The formation of NaMnF<sub>3</sub> nanocubes strongly depends on the ethanol solvent. The morphology and single-phase of obtained samples could be well maintained by controlling the doping concentration (Yb<sup>3+</sup> ≤ 20 mol%). Single-band red upconversion emission can be generated in Er<sup>3+</sup>/Yb<sup>3+</sup> codoped NaMnF<sub>3</sub> nanocubes due to the energy transfer between host Mn<sup>2+</sup> and dopant Er<sup>3+</sup> ions. It is revealed that our NaMnF<sub>3</sub>:Er<sup>3+</sup>/Yb<sup>3+</sup> nanocubes irradiate the brightest red luminescence at the dopant concentrations of Er<sup>3+</sup> (2 mol%) and Yb<sup>3+</sup> (15 mol%), which is stronger than that of hexagonal-phase NaYF<sub>4</sub>:Er<sup>3+</sup>/Yb<sup>3+</sup> phosphor.

<sup>a</sup>Department of Mechanical Engineering, Iowa State University, Ames, IA 50011, USA. E-mail: [nastaran@iastate.edu](mailto:nastaran@iastate.edu)

<sup>b</sup>Department of Electrical and Electronic Engineering, Graduate School of Engineering, Kobe University, Rokkodai, Nada, Kobe 657-8501, Japan

## 1. Introduction

The development of upconversion (UC) phosphors has received considerable attention owing to their applications in solid-state lasers, optical data storage, illumination, color display, and biological labeling.<sup>1-3</sup> Especially as a biological labeling material, UC fluorescent labels show very low background light as a result of their unique fluorescence properties and high detection limits compared with their traditional counterparts, such as organic dyes and quantum dots.<sup>4,5</sup> The most efficient UC phosphor currently known is based on  $\text{Er}^{3+}$  ion in combination with  $\text{Yb}^{3+}$  ion as a sensitizer, which exhibits a green emission ( $\sim 550$  nm) as well as a red emission ( $\sim 660$  nm).<sup>6</sup> The red emission is of technological importance since it is located in the “optical transmission window” of biological tissues, which has the minimum absorption of tissues and the maximum penetration depth.<sup>7</sup> On the other hand, the green emission cannot effectively penetrate the deep tissue and may also cause many unwanted side effects that will reduce the sensitivity of the imaging.<sup>8</sup> Therefore, avoiding the green emission and achieving strong and single-band red emission from  $\text{Er}^{3+}$  -  $\text{Yb}^{3+}$  couple is eagerly demanded for the development of high-sensitivity and high-specificity probes for bioimaging.

Recently,  $\text{Mn}^{2+}$ -based nanocrystals have been known as ideal host materials to achieve single-band UC emission from  $\text{Er}^{3+}$  ions because of the energy transfer between the  $\text{Er}^{3+}$  and  $\text{Mn}^{2+}$ .<sup>9-11</sup> Up to now, some approaches have been developed for the preparation of various  $\text{Mn}^{2+}$ -based nanocrystals including  $\text{MnF}_2$ ,  $\text{KMnF}_3$  and  $\text{NaMnF}_3$ .<sup>12-14</sup> It is well established that the shape and size of the material strongly affect the properties and the applications of the material.<sup>15-19</sup> Hence, much effort has been dedicated on controlling the size and shape of the particles.<sup>10,20</sup> However, in most cases, the geometry of  $\text{Mn}^{2+}$ -based nanostructures obtained by conventional hydro/solvo-thermal method is spherical, and the synthesis of non-spherical nanostructures still suffers from extra technological difficulties.<sup>11,13,14</sup> In addition, the previously reported approaches still suffer from problems including complicated experimental conditions, tedious procedures, and high reaction temperatures ( $\geq 160$  °C).<sup>10,12</sup> Hence, from safety and energy-saving viewpoints, it is

highly desirable to develop a novel low-temperature solution-phase synthesis protocol to manipulate the morphology of  $\text{Mn}^{2+}$ -based nanostructures.

In the present work, we have developed a straightforward wet-chemical approach to fabricate uniform and monodispersed  $\text{Er}^{3+}/\text{Yb}^{3+}$  codoped  $\text{NaMnF}_3$  nanocubes. The effects of the reaction temperature, and the volume ratio between ethanol and DI water on the morphology of  $\text{NaMnF}_3$  nanocubes are systematically investigated. We examine the structural and UC luminescence properties of the  $\text{NaMnF}_3:\text{Er}^{3+}/\text{Yb}^{3+}$  nanocubes as a function of dopant concentrations of  $\text{Er}^{3+}/\text{Yb}^{3+}$  (1~3 : 5~20 mol%). The UC luminescence properties of as-prepared nanocubes are compared with those of hexagonal-phase  $\text{NaYF}_4$  with the same dopant concentrations.

## 2. Experimental

### 2.1. Sample preparation

$\text{NaF}$  (99 %),  $\text{MnCl}_2 \cdot 4\text{H}_2\text{O}$  (99 %),  $\text{YbCl}_3 \cdot 6\text{H}_2\text{O}$  (99.9 %),  $\text{ErCl}_3 \cdot 6\text{H}_2\text{O}$  (99.9 %), and absolute ethanol were purchased from Sigma-Aldrich and were used as starting materials without further purification. DI water is used as solvent for the above chemicals to prepare stock solution. The strategy for synthesizing  $\text{Er}^{3+}/\text{Yb}^{3+}$  codoped  $\text{NaMnF}_3$  nanocubes is schematically depicted in scheme 1. In a typical synthesis process,  $\text{NaMnF}_3$  doped with 2 mol%  $\text{Er}^{3+}$  and 20 mol%  $\text{Yb}^{3+}$  was synthesized as follows: 3.12 mL of 0.2 M  $\text{MnCl}_2 \cdot 4\text{H}_2\text{O}$ , 0.8 mL of 0.2 M  $\text{YbCl}_3 \cdot 6\text{H}_2\text{O}$  and 0.08 mL of 0.2 M  $\text{ErCl}_3 \cdot 6\text{H}_2\text{O}$ , and 4 mL of 0.6 M  $\text{NaF}$  were sequentially added to a beaker containing 24 mL of absolute ethanol under vigorous stirring. The reaction temperatures were set to be room temperature (25 °C), 50 °C and 80 °C, according to the experiment requirements. The final products were collected by means of centrifugation, washed with DI water for several times.

### 2.2. Characterization

The crystal structure of prepared products was analyzed by an X-ray powder diffractometer (Rigaku-TTR/S2) using  $\text{CuK}\alpha$  radiation ( $\lambda = 1.54056 \text{ \AA}$ ). The size and morphology of the products were

examined by using a field emission scanning electron microscope (FE-SEM, JSM-6700F at an acceleration voltage of 5 kV) equipped with an energy dispersive X-ray spectroscopy (EDX, Horiba 7593-H model). The UC luminescence spectra were recorded using a fluorescence spectrophotometer (Horiba Jobin Yvon FluoroLog3) in conjunction with a 980-nm laser as the excitation source. All measurements were performed at room temperature.

### 3. Results and discussion

#### 3.1. Characterizations of structure and morphology

The synthesis of  $\text{NaMnF}_3$  materials is performed in various methods to study the effects of the experiment parameters such as reaction temperature, solvent and dopant. Fig. 1a presents the XRD patterns of  $\text{NaMnF}_3$  host materials synthesized at various reaction temperatures. It can be seen that all the diffraction peaks of the samples correspond to the  $\text{NaMnF}_3$  crystal (JCPDS standard card no. 18-1224). The similar diffraction patterns of all samples reveal that the  $\text{NaMnF}_3$  crystal can be formed in the temperature range of 25~80 °C. The sharp and strong peaks of  $\text{NaMnF}_3$  crystals suggest high crystallinity of the obtained samples. The XRD patterns of  $\text{NaMnF}_3$ : 2 mol%  $\text{Er}^{3+}$ , (10~30) mol%  $\text{Yb}^{3+}$  phosphors are also shown in Fig. 1b. It is evidenced that the crystal structure keeps the same until the  $\text{Yb}^{3+}$  concentration reaches 20 mol%, indicating that doped elements have been effectively doped into the host lattice. It is notable that an impurity phase is developed for the  $\text{NaMnF}_3$ : 2 mol%  $\text{Er}^{3+}$ , 30 mol%  $\text{Yb}^{3+}$  sample, which can be assigned to the  $\text{Na}_5\text{Yb}_9\text{F}_{32}$  crystal (JCPDS standard card no. 27-1426).

The morphology of  $\text{NaMnF}_3$  host obtained at different reaction temperatures is characterized by SEM. From the low-resolution SEM images (Fig. 2a-c), uniform and monodispersed nanocubes with an average size around 900 nm can be obtained in the reaction temperature range of 25~80 °C. As revealed by the magnified SEM image (Fig. 2d), the surfaces of nanocubes are very rough, and full of cracks are observed when the reaction is carried out at room temperature. With the increase of reaction temperature to 50 °C, the cracks are gradually disappeared (Fig. 2e), and finally, very smooth surface over the whole

particle is obtained at 80 °C (Fig. 2f). The morphology of NaMnF<sub>3</sub> host is also investigated by doping various amounts of rare-earth ions. As shown in Fig. 3(a and b), the morphologies of Er<sup>3+</sup>/Yb<sup>3+</sup> codoped NaMnF<sub>3</sub> nanocrystals are kept well until the Yb<sup>3+</sup> doping concentration reaches 20 mol%. However, for the higher Yb<sup>3+</sup> doping (30 mol%), besides the nanocubes, the coexistence of nanoparticles with the size of 100 nm is observed (Fig. 3c). It is confirmed that these nanoparticles are responsible for the impurity phase shown in Fig. 1b, which indicates that the excessive Yb<sup>3+</sup> ions in solution prefer to react with NaF to form Na<sub>5</sub>Yb<sub>9</sub>F<sub>32</sub> crystal, rather than doped into NaMnF<sub>3</sub> host. Based on the both XRD and SEM results, doping Yb<sup>3+</sup> ion lower than 20 mol% is essential to preserve the single-phase and morphology of obtained samples.

Reaction solvent is another critical factor for the growth of nanocrystals, which can influence the reaction rate of crystal formation and further determine the phase and morphology of the final products.<sup>21,22</sup> To evaluate the effect of reaction solvent on the formation of obtained samples, a set of NaMnF<sub>3</sub> nanocrystals are fabricated in the mixed solutions of ethanol (ET) and DI water (DW). The sum amount of ethanol and DI water was fixed to 24 mL, and the ET/DW volume ratio was varied to 0:24 mL, 8:16 mL, 16:8 mL, and 24:0 mL. As shown in Fig. 4a, with the solvent of DI water, the irregularly-shaped and strongly-aggregated large blocks (several micrometers) as well as nanoparticles (~100 nm) can be produced. With the addition of ethanol (8 mL) into solvent, the formation of aggregated micro-clusters and micro-hexahedrons with large size distributions are confirmed (Fig. 4b). In the solvent with 16 mL ethanol, the micro-clusters are disappeared, and irregular hexahedrons with the size range of 1~2 μm are observed (Fig. 4c). When the reaction is carried out in absolute ethanol, monodispersed nanocubes with a size of about 900 nm can be obtained (Fig. 4d). The results reveal that the introduction of ethanol in reaction system can effectively prevent agglomeration and stimulate the growth into NaMnY<sub>3</sub> nanocubic assemblies.

The variation of ethanol content has a great influence on the morphology of various nanomaterials, such as SiO<sub>2</sub> and BaSO<sub>4</sub>.<sup>23-25</sup> For instance, it was reported that the size of BaSO<sub>4</sub> is reduced from 85 nm to 54 nm with the increase of ethanol percentage in ethanol-water mixed solvent from 30 % to 70 %.<sup>24</sup> The

effect of water and ethanol amount on the morphology of  $\text{NaMnF}_3$  could be attributed to the solvent interactions with the precursors, manganese chloride and sodium fluoride.<sup>26</sup> It is well known that water has higher degree of porosity than ethanol. Increasing the ET/DW ratio will decrease the solvent polarity and the interfacial energy with the particles, which prevents the aggregation of the particles due to water swelling effect and makes the system more homogeneous.<sup>27,28</sup> On the other hand, the reason for the formation of cubic particles may lie in an unusual inherent characteristic of  $\text{NaMnF}_3$ .<sup>29</sup> The ethanol solvent with relatively longer chain than water may change the order of the free energies of different facets through their interactions with the specific facets of  $\text{NaMnF}_3$  crystals.<sup>30</sup> This alternation may significantly affect the relative growth rates of different facets and lead to the crystals with cubic morphology.

### 3.2. Upconversion luminescence properties

Fig. 5(a and b) show the room-temperature UC emission spectra of  $\text{NaMnF}_3$  nanocubes doped with various concentrations of  $\text{Er}^{3+}$  and  $\text{Yb}^{3+}$  ions. In comparison with  $\text{Er}^{3+}/\text{Yb}^{3+}$  codoped routine rare-earth based fluoride nanocrystals which typically exhibit multiple-band emissions in the visible spectral region, a single-band emission in the spectral range of 640~690 nm is detected for all the  $\text{NaMnF}_3$  nanocubes doped with different amount of  $\text{Er}^{3+}/\text{Yb}^{3+}$  (1~3 : 5~20 mol%) upon excitation at 980 nm, which is assigned to the  $^4\text{F}_{9/2} \rightarrow ^4\text{I}_{15/2}$  transition of  $\text{Er}^{3+}$  ions. It should be noted that though single-band red emission has been realized in several host materials, it is still challenging to obtain red emission with the high chromatic purity in  $\text{NaMnF}_3$  host.<sup>31,32</sup> In  $\text{NaMnF}_3$  nanocubes, the red-to-green intensity ratios in all samples are larger than 40, which indicate that the present materials are favorable for applications in deep-tissue bioimaging (Fig. S1). In addition, the full width at half maximum (FWHM) of the red-emitting band is measured to be 27 nm, which is comparable to that for  $\text{KMnF}_3:\text{Yb}^{3+}/\text{Er}^{3+}$  nanocrystals (20 nm), but is narrower than the red emission bands of  $\text{ZrO}_2:\text{Yb}^{3+}/\text{Er}^{3+}$  nanocrystals (42 nm) or  $\text{Y}_2\text{O}_3:\text{Yb}^{3+}/\text{Er}^{3+}$  nanocrystals (75 nm).<sup>10,33,34</sup>

To gain more information on the UC mechanism, the pumping power dependence of UC luminescence intensity is studied. For an unsaturated UC process, the UC emission intensity ( $I$ ) increases in

proportion to the excitation power ( $P$ ) according to the power law  $I \propto P^x$ , and generally, the measured slope of  $x$  is indicative of an upconversion process, which involves at least  $n$  photons, where  $n$  is the smallest integer greater than  $x$  or equal to  $x$  if  $x$  is an integer.<sup>35,36</sup> Fig. 5c shows the log-log plots of the red luminescence intensity in 2 mol% Er<sup>3+</sup>/20 mol% Yb<sup>3+</sup> doped NaMnF<sub>3</sub> nanocubes as a function of excitation intensity at 980 nm. The result indicates that, a slope  $n$  value of 1.83 is obtained for the red emission band, indicating that two-photon processes are involved for generating the UC emissions in the present sample. It is also noteworthy that, the single-band feature of Er<sup>3+</sup>/Yb<sup>3+</sup> codoped NaMnF<sub>3</sub> can be remained well in the broad excitation power density range of 7.5~20 mW/cm<sup>2</sup> (Fig. S2).

According to the energy matching and quadratic dependence on excitation power, the possible UC mechanisms for the single-band red emission are discussed based on the simplified energy levels of Er<sup>3+</sup>, Yb<sup>3+</sup> and Mn<sup>2+</sup> ions. As illustrated in Fig. 5d, the Er<sup>3+</sup> ion can be firstly excited to the <sup>4</sup>I<sub>11/2</sub> state through an energy transfer process from a Yb<sup>3+</sup> ion, and then further jumped to the <sup>4</sup>F<sub>7/2</sub> state by absorbing the energy from another Yb<sup>3+</sup> ion. Then Er<sup>3+</sup> ion can be nonradiatively relaxed to two lower levels, <sup>2</sup>H<sub>11/2</sub> and <sup>4</sup>S<sub>3/2</sub>, resulting in the green (<sup>2</sup>H<sub>11/2</sub> → <sup>4</sup>I<sub>15/2</sub> and <sup>4</sup>S<sub>3/2</sub> → <sup>4</sup>I<sub>15/2</sub>) UC emissions, and even further relaxed to <sup>4</sup>F<sub>9/2</sub> level to generate red (<sup>4</sup>F<sub>9/2</sub> → <sup>4</sup>I<sub>15/2</sub>) emission. However, with the presence of large amount of Mn<sup>2+</sup> ions in NaMnF<sub>3</sub> host, the interaction between Er<sup>3+</sup> and Mn<sup>2+</sup> plays an important role on modifying the UC emissions. Due to the close proximity and excellent overlap of energy levels of the Er<sup>3+</sup> and Mn<sup>2+</sup> ions in the host lattices, a nonradiative energy transfer from the <sup>2</sup>H<sub>11/2</sub> and <sup>4</sup>S<sub>3/2</sub> levels of Er<sup>3+</sup> to the <sup>4</sup>T<sub>1</sub> level of Mn<sup>2+</sup>, which is followed by back-energy transfer to the <sup>4</sup>F<sub>9/2</sub> level of Er<sup>3+</sup>.<sup>10,31</sup> The large red-to-green intensity ratios in all samples suggests that an extremely efficient exchange-energy transfer process occurs between the Er<sup>3+</sup> and Mn<sup>2+</sup> ions.

As is known, the luminescence intensity from rare-earth ions strongly depends on the doping level, and the proper doping is indispensable to achieve maximum intensity.<sup>9,37</sup> The UC luminescence intensities are compared between the NaMnF<sub>3</sub> nanocubes doped with various concentrations of Er<sup>3+</sup> and Yb<sup>3+</sup> ions (Fig.



S3). In the condition of 20 mol%  $\text{Yb}^{3+}$  in  $\text{NaMnF}_3$  nanocubes, the sample with  $\text{Er}^{3+}$ : 2 mol% irradiates brightest red luminescence, which indicates that the further increase of  $\text{Er}^{3+}$  concentration does not benefit luminescence intensity. In the previous publication, Du *et al.* reported that, the optimum  $\text{Er}^{3+}$  concentration in  $\text{Ca}_{0.65}\text{La}_{0.35}\text{F}_{2.35}$  host should be 2 mol%, which is consistent with our results.<sup>38</sup> On the other hand, with 2 mol%  $\text{Er}^{3+}$  concentration, the red emission increases with the  $\text{Yb}^{3+}$  concentration increases from 5 mol% to 15 mol%, and further increase of  $\text{Yb}^{3+}$  concentration results in the decrease of red emission due to concentration quenching effect.<sup>20</sup> The above comparative studies suggest that our  $\text{NaMnF}_3:\text{Er}^{3+}/\text{Yb}^{3+}$  nanocrystals fabricated by present synthetic procedure own the strongest single-band emission feature at the dopant concentrations of  $\text{Er}^{3+}$  (2 mol%) and  $\text{Yb}^{3+}$  (15 mol%).

It should be noted that, in the previously published paper, Zhang *et al.* synthesized  $\text{Er}^{3+}/\text{Yb}^{3+}$  doped  $\text{NaMnF}_3$  nanocrystals in the mixed solvents of 1-octadecene and oleic acid at 300 °C, and the strongest emission appears at  $\text{Er}^{3+}$  (25 mol%) and  $\text{Yb}^{3+}$  (25 mol%).<sup>11</sup> In contrast, in our samples fabricated in ethanol at 80 °C, the dopant ions ( $\text{Er}^{3+} + \text{Yb}^{3+}$ ) cannot reach very high level ( $\leq 22\%$ ), since the excessive  $\text{Yb}^{3+}$  ions in ethanol prefer to react with NaF to form  $\text{Na}_5\text{Yb}_9\text{F}_{32}$  crystal, rather than doped into  $\text{NaMnF}_3$  host. The dopant ions can occupy the  $\text{Mn}^{2+}$  sites in the host crystals. It is reasonable to assume that, some  $\text{Mn}^{2+}$  sites are favourable for dopant ions when fabricated by our method. With the increase of reaction temperature, the dopants may occupy more  $\text{Mn}^{2+}$  sites. Therefore, the distance and interaction between dopants are different in samples fabricated by different methods, which results in distinct luminescence properties.

Among the investigated fluorides, hexagonal-phase  $\text{NaYF}_4$  is known as one of the most efficient host lattices for both downconversion and UC processes.<sup>39,40</sup> To evaluate the luminescence efficiency of  $\text{NaMnF}_3$  host, a reference sample, hexagonal-phase  $\text{NaYF}_4$  doped with 2 mol%  $\text{Er}^{3+}$  and 15 mol%  $\text{Yb}^{3+}$  has been prepared by a modified version of the procedure described previously (Fig. S4).<sup>41,42</sup> Fig. 6 shows the comparison of UC luminescence spectra of  $\text{NaYF}_4$  and  $\text{NaMnF}_3$  doped with 2 mol%  $\text{Er}^{3+}$  and 15 mol%  $\text{Yb}^{3+}$  ions, respectively. The same amounts of samples are measured at the same experimental condition. Under

the 980 nm excitation, the NaYF<sub>4</sub> sample shows multi-peak emissions in the green and red regions, though pure red emission is detected from NaMnF<sub>3</sub> sample. Despite the emission difference, the red emission intensity of NaMnF<sub>3</sub>:Er<sup>3+</sup>/Yb<sup>3+</sup> is 1.4 times stronger and overall (green-plus-red) emissions are 1.2 times greater than those of NaYF<sub>4</sub>:Er<sup>3+</sup>/Yb<sup>3+</sup> sample, indicating that NaMnF<sub>3</sub> is a promising host material for deep tissue bioimaging. Such a red-emission enhancement should mostly arise from the efficient cross-relaxation of energy between Mn<sup>2+</sup> and Er<sup>3+</sup> ions.

#### 4. Conclusions

In summary, we have demonstrated the fabrication of uniform and monodispersed NaMnF<sub>3</sub> nanocubes by a facile low-temperature solution-based method at ambient conditions. It is revealed that the proper controlling of the reaction temperature and solvent is critical for the formation of NaMnF<sub>3</sub> nanocubes. Though the NaMnF<sub>3</sub> nanocubes can be formed in the temperature range of 25~80 °C, higher temperature is favorable to obtain uniform and smooth products. The ethanol solvent is essential for the formation of NaMnF<sub>3</sub> nanocubic assemblies. Doping Yb<sup>3+</sup> ion lower than 20 mol% is required to preserve the single-phase and morphology of obtained materials. As a result of efficient energy transfer between the dopant Er<sup>3+</sup> ion and host Mn<sup>2+</sup> ion, remarkably pure red UC emissions were generated in the dopant concentration ranges of Er<sup>3+</sup>/Yb<sup>3+</sup> (1~3 : 5~20 mol%). The strongest red emission in these Er<sup>3+</sup>/Yb<sup>3+</sup> doped nanocrystals has been realized at the dopant concentrations of Er<sup>3+</sup> (2 mol%) and Yb<sup>3+</sup> (15 mol%). The achieved red emission is 1.4 times stronger and overall (green-plus-red) emissions are 1.2 times greater than those of NaYF<sub>4</sub>:Er<sup>3+</sup>/Yb<sup>3+</sup> phosphor.

#### Acknowledgements

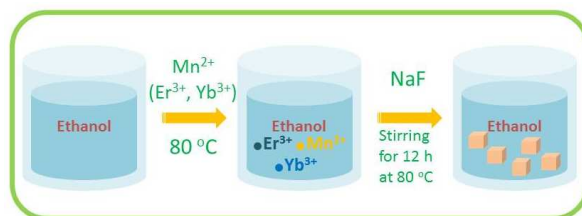
We gratefully acknowledge the William March Scholar program and the Iowa State University Presidential Initiative for Interdisciplinary Research and Health Research Initiative (ISU-HRI) for support of this work.

**References**

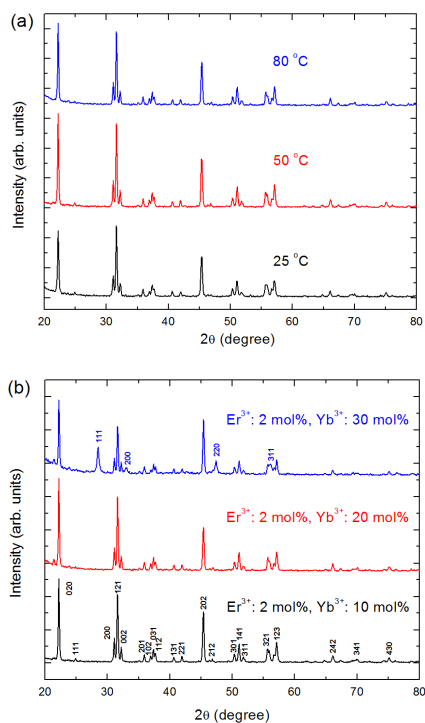
1. M. Ito, C. Goutaudier, Y. Guyot, K. Lebbou, T. Fukuda and G. Boulon, *J. Phys.: Condens. Matter*, 2004, **16**, 1501-1521.
2. H. T. Sun, C. L. Yu, Z. C. Duan, L. Wen, J. J. Zhang, L. L. Hu and S. X. Dai, *Opt. Mater*, 2006, **28**, 448-452.
3. L. Q. Xiong, Z. G. Chen, Q. W. Tian, T. Y. Cao, C. J. Xu and F. Y. Li, *Anal Chem*, 2009, **81**, 8687-8694.
4. S. A. Hilderbrand, F. W. Shao, C. Salthouse, U. Mahmood and R. Weissleder, *Chem Commun*, 2009, **28**, 4188-4190.
5. H. S. Mader, P. Kele, S. M. Saleh and O. S. Wolfbeis, *Curr Opin Chem Biol*, 2010, **14**, 582-596.
6. F. Vetrone, J. C. Boyer, J. A. Capobianco, A. Speghini and M. Bettinelli, *J. Appl. Phys*, 2004, **96**, 661-667.
7. K. Konig, *J Microsc-Oxford*, 2000, **200**, 83-104.
8. G. Tian, Z. J. Gu, X. X. Liu, L. J. Zhou, W. Y. Yin, L. Yan, S. Jin, W. L. Ren, G. M. Xing, S. J. Li and Y. L. Zhao, *J Phys Chem C*, 2011, **115**, 23790-23796.
9. Z. H. Bai, H. T. Sun, T. Hasegawa, M. Fujii, F. Shimaoka, Y. Miwa, M. Mizuhata and S. Hayashi, *Opt Lett*, 2010, **35**, 1926-1928.
10. J. Wang, F. Wang, C. Wang, Z. Liu and X. G. Liu, *Angew. Chem. Int. Ed*, 2011, **50**, 10369-10372.
11. Y. Zhang, J. D. Lin, V. Vijayaragavan, K. K. Bhakoo and T. T. Y. Tan, *Chem Commun*, 2012, **48**, 10322-10324.
12. J. H. Zeng, T. Xie, Z. H. Li and Y. D. Li, *Cryst Growth Des*, 2007, **7**, 2774-2777.
13. M. Li, X. F. Yu, W. Y. Yu, J. Zhou, X. N. Peng and Q. Q. Wang, *J Phys Chem C*, 2009, **113**, 20271-20274.
14. M. Y. Xie, X. N. Peng, X. F. Fu, J. J. Zhang, G. L. Lia and X. F. Yu, *Scr. Mater*, 2009, **60**, 190-193.

15. J. H. Zeng, J. Su, Z. H. Li, R. X. Yan and Y. D. Li, *Adv. Mater.*, 2005, **17**, 2119-2123.
16. C. X. Li, Z. W. Quan, J. Yang, P. P. Yang and J. Lin, *Inorg Chem*, 2007, **46**, 6329-6337.
17. R. Montazami, S. Liu, Y. Liu, D. Wang, Q. Zhang, J. R. and Heflin, *J Appl Phys* 2011, 109, 104301.
18. R. Montazami, C. M. Spillmann, J. Naciri, and B. R. Ratna, *Sens Actuators A* 2012, 178, 175.
19. R. Montazami, D. Wang, and J. R. Heflin, *Int J Smart and Nano Materials* 2012, 3, 204.
20. Z. Bai, H. Lin, J. Johnson, S. C. Rong Gui, K. Imakita, R. Montazami, M. Fujii and N. Hashemi, *J Mater Chem C*, 2014, **2**, 1736-1741.
21. K. W. Kramer, D. Biner, G. Frei, H. U. Gudel, M. P. Hehlen and S. R. Luthi, *Chem. Mater.*, 2004, **16**, 1244-1251.
22. H. X. Mai, Y. W. Zhang, R. Si, Z. G. Yan, L. D. Sun, L. P. You and C. H. Yan, *J. Am. Chem. Soc.*, 2006, **128**, 6426-6436.
23. K.S. Rao, K.E. Hami, T. Koday, K. Matsushigue and K. Makino, *J. Colloid Interface Sci.* 2005, **289** 125–131.
24. V. Ramaswamy, R. M. Vimalathithan and V. Ponnusamy, *J. Ceram Process Res.* 2011, **12**, 173-175.
25. X. Zhang, Y. Li and C. Cao, *J. Mater. Chem.*, 2012, **22**, 13918-13921.
26. P. B. Khoza, M. J. Moloto and L. M. Siklrwivhilu, *J. Nanotechnol.* 2012, 2012.
27. C. J. Kim and M. S. Kwon, *Electron. Mater. Lett.* 2009, **5**, 113-117.
28. M. Thirumavalavan, K. L. Huang and J. F. Lee, *Mater.* 2013, **6**, 4198-4212.
29. L. Qi, J. Ma, H. Cheng and Z. Zhao, *Colloids Surfaces A: Physicochem. Eng. Aspects*, 1996, **108**, 117-126.
30. S. Tanvir and L. Qiao, *Nanoscale Res Lett*, 2012, **7**, 226.
31. G. Tian, Z. J. Gu, L. J. Zhou, W. Y. Yin, X. X. Liu, L. Yan, S. Jin, W. L. Ren, G. M. Xing, S. J. Li and Y. L. Zhao, *Adv. Mater.*, 2012, **24**, 1226-1231.
32. Z. H. Bai, M. Fujii, K. Imakita and S. Hayashi, *Micro. Meso. Mater.*, 2013, **173**, 43-46.

33. D. Matsuura, *Appl Phys Lett*, 2002, **81**, 4526-4528.
34. G. Y. Chen, Y. G. Zhang, G. Somesfalean, Z. G. Zhang, Q. Sun and F. P. Wang, *Appl Phys Lett*, 2006, **89**, 163105.
35. M. Pollnau, D. R. Gamelin, S. R. Luthi, H. U. Gudel and M. P. Hehlen, *Phys Rev B*, 2000, **61**, 3337-3346.
36. H. T. Sun, L. L. Hu, C. L. Yu, G. Zhou, Z. C. Duan, J. J. Zhang and Z. H. Jiang, *Chem Phys Lett*, 2005, **408**, 179-185.
37. Z. H. Bai, M. Fujii, Y. Mori, Y. Miwa, M. Mizuhata, H. T. Sun and S. Hayashi, *Opt Lett*, 2011, **36**, 1017-1019.
38. P. Du, Z. Xia and L. Liao, *Mater. Res. Bull.*, 2011, **46**, 543-546.
39. F. Wang and X. G. Liu, *J. Am. Chem. Soc.*, 2008, **130**, 5642-5643.
40. G. Y. Chen, T. Y. Ohulchanskyy, R. Kumar, H. Agren and P. N. Prasad, *Acs Nano*, 2010, **4**, 3163-3168.
41. G. S. Yi, H. C. Lu, S. Y. Zhao, G. Yue, W. J. Yang, D. P. Chen and L. H. Guo, *Nano Letters*, 2004, **4**, 2191-2196.
42. G. Y. Chen, H. C. Liu, G. Somesfalean, H. J. Liang and Z. G. Zhang, *Nanotechnology*, 2009, **20**, 385704.

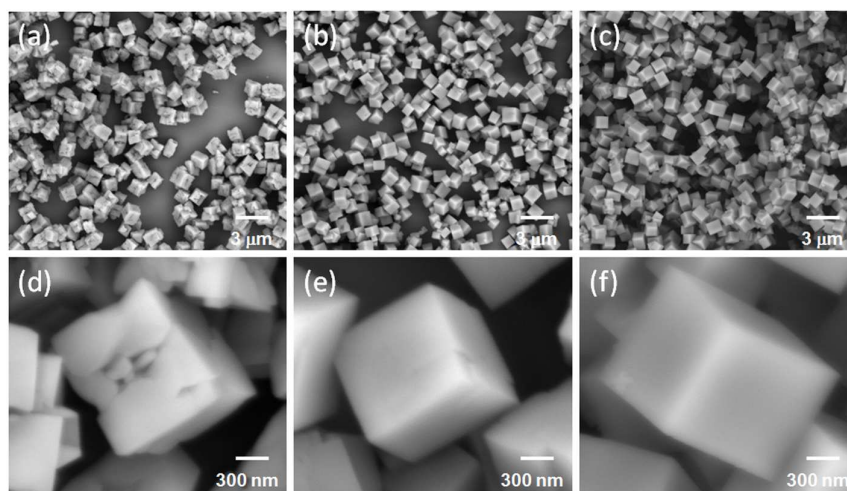


**Scheme 1** Schematic illustration of the fabrication strategy for Er<sup>3+</sup>/Yb<sup>3+</sup> codoped NaMnF<sub>3</sub> nanocubes.



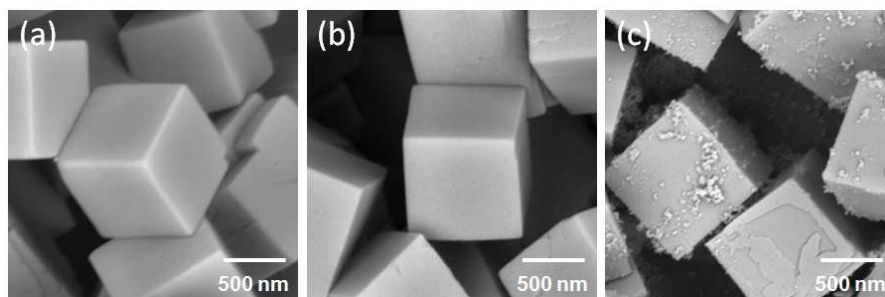
**Fig. 1** (a) XRD patterns of NaMnF<sub>3</sub> particles synthesized at the reaction temperature range of 25~80 °C. (b)

XRD patterns of NaMnF<sub>3</sub> nanostructures (80 °C) doped with 2 mol% Er<sup>3+</sup> and (10~30) Yb<sup>3+</sup> ions.

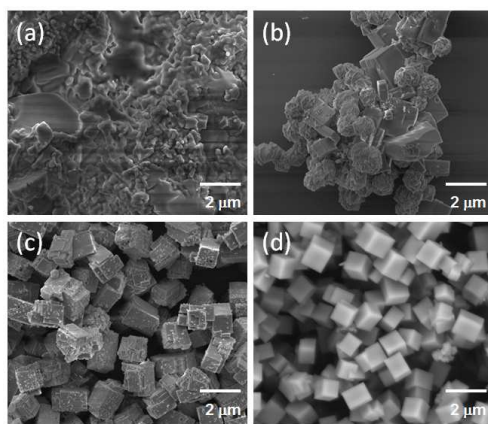


**Fig. 2** Low-resolution and high-resolution SEM images of NaMnF<sub>3</sub> nanocrystals synthesized at various reaction temperatures: (a) and (d) 25 °C; (b) and (e) 50 °C; (c) and (f) 80 °C, respectively.

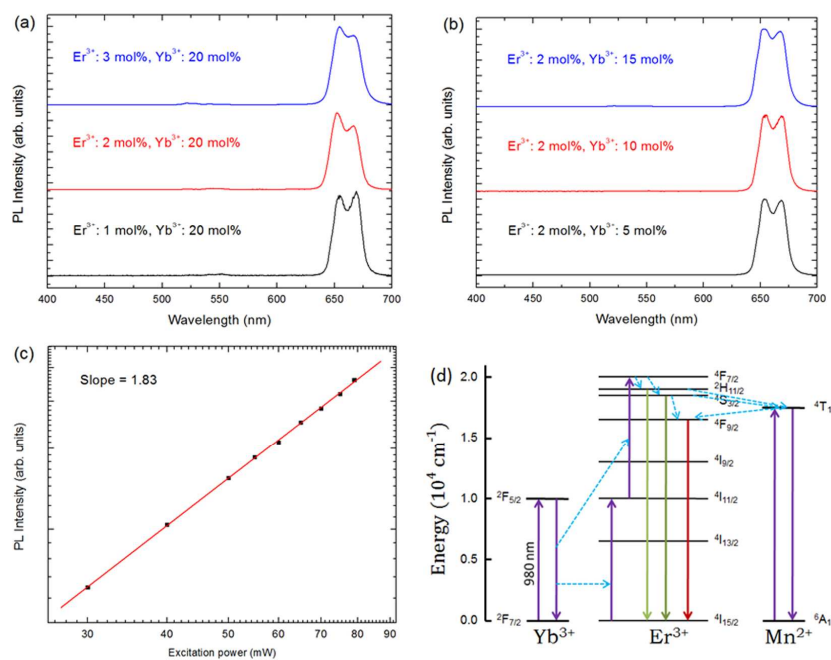




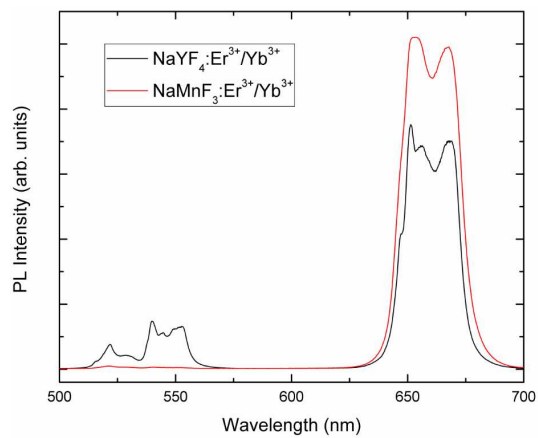
**Fig. 3** SEM images of  $\text{NaMnF}_3$  nanocubes doped with 2 mol%  $\text{Er}^{3+}$  and  $\text{Yb}^{3+}$  of (a) 10 mol%, (b) 20 mol% and (c) 30 mol%.



**Fig. 4** SEM images of  $\text{NaMnF}_3$  nanostructures synthesized by various volume ratios of ethanol to water: (a) 0:24 mL; (b) 8:16 mL; (c) 16:8 mL; (d) 24:0 mL.

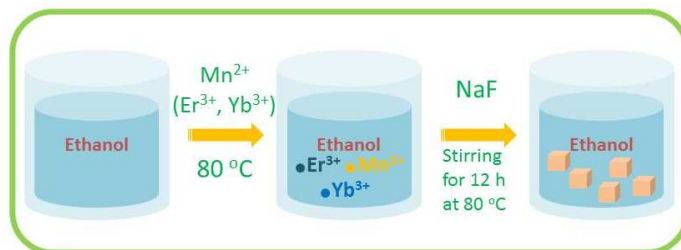


**Fig. 5** (a and b) Normalized upconversion luminescence spectra of NaMnF<sub>3</sub> nanocubes doped with various concentrations of Er<sup>3+</sup>/Yb<sup>3+</sup> (1~3 : 5~20 mol%). (c) Log-log plots of the red emission intensity versus excitation power in 2 mol% Er<sup>3+</sup>/20 mol% Yb<sup>3+</sup> codoped NaMnF<sub>3</sub> nanocubes. (d) Simplified energy level diagrams of Er<sup>3+</sup>, Yb<sup>3+</sup> and Mn<sup>2+</sup> ions and possible transition pathways in NaMnF<sub>3</sub>.



**Fig. 6** Comparison of upconversion luminescence spectra of hexagonal-phase NaYF<sub>4</sub> and NaMnF<sub>3</sub> host nanocrystals doped with 2 mol% Er<sup>3+</sup> and 15 mol% Yb<sup>3+</sup> ions, respectively.

## For Table of Content Entry



A facile synthetic method has been developed for fabrication of Er<sup>3+</sup>/Yb<sup>3+</sup> codoped NaMnF<sub>3</sub> nanocubes, which show pure red emission.